Stress-induced catecholamines attenuate sorafenib efficacy by inhibiting ferroptosis in β2-adrenergic receptor positive renal cell carcinoma

MASAKI USHIJIMA[1], SEI NAITO[1], HIROMI ITO[1], TAKAFUMI NARISAWA[1], OSAMU ICHIYANAGI[1], HIDENORI KANNO[1], HIROKI FUKUHARA[1], YUKI TAKAI[1], MAYU YAGI[1], ATUSHI YAMAGISHI[1], HAYATO NISHIDA[1], YUTARO OBARA[2] and NORIHIKO TSUCHIYA[1]

[1]Department of Urology, Yamagata University Faculty of Medicine, Yamagata 990-9585, Japan; [2]Department of Pharmacology, Yamagata University Faculty of Medicine, Yamagata 990-9585, Japan

Received October 15, 2025; Accepted March 6, 2026

DOI: 10.3892/ijo.2026.5905

Abstract. Ferroptosis, an iron-dependent form of non-apoptotic cell death, is a potential target for cancer therapy. Sorafenib, a molecular targeted agent for renal cell carcinoma (RCC), is involved in ferroptosis induction. Chronic stress, mediated by catecholamines via β2-adrenergic receptors (ADRB2), promotes cancer progression, yet its influence on drug resistance and ferroptosis remains elusive. To investigate ADRB expression in RCC, immunohistochemistry of surgical specimens was performed and assessed ADRB mRNA and protein levels were assessed by RT-qPCR and western blotting in RCC cell lines. To determine whether β-adrenergic signaling modulates sorafenib sensitivity, we used ADRB2-expresing ACHN cells and conducted MTS cell viability assays following β-adrenergic agonist isoproterenol (ISO) stimulation, ADRB2 knockdown by siRNA, as well as a restraint-stress mouse model in which catecholamine levels were elevated, bearing ACHN cells or ACHN cells with ADRB2 knockdown by shRNA. To evaluate the involvement of ferroptosis, we applied the ferroptosis inhibitor ferrostatin-1 (Fer-1) and inducers erastin and RSL3, and measured cell viability, malondialdehyde and reactive oxygen species. To elucidate the mechanism underlying the ISO effect on ferroptosis, MAPK pathway activity was assessed by western blotting and MTS assays performed under MAPK inhibition. The present study confirmed ADRB2 expression in RCC by immunohistochemistry of surgical specimens. Using the ADRB2-expressing RCC cell line ACHN, the present study demonstrated that stimulation with the β-adrenergic agonist isoproterenol (ISO) conferred resistance to sorafenib both *in vitro* and in a mouse stress model; this effect was abrogated by ADRB2 knockdown. Similarly to ISO, Fer-1 diminished sorafenib sensitivity in ACHN cells. Erastin and RSL3 markedly decreased cell viability, however, ISO attenuated ferroptosis in ACHN cells. Mechanistically, ISO inhibited the phosphorylation of ERK1/2, p38 and JNK, all of which contribute to ferroptosis suppression. These findings provide evidence that chronic stress-induced ADRB2 activation promotes sorafenib resistance by mitigating ferroptotic cell death.

Correspondence to: Dr Sei Naito, Department of Urology, Yamagata University Faculty of Medicine, 2-2-2 Iida-nishi, Yamagata 990-9585, Japan
E-mail: seinaito@med.id.yamagata-u.ac.jp

Abbreviations: ADRB1, β1-adrenergic receptor; ccRCC, clear cell renal cell carcinoma; Fer-1, ferrostatin-1; GPX4, glutathione peroxidase 4; GSH, glutathione; HPA; hypothalamic-pituitary-adrenal; ICGC, International Cancer Genome Consortium; IHC, immunohistochemical; ISO, isoproterenol; 3-MA, 3-methyladenin; MDA, malondialdehyde; MTD, molecular targeted drug; Nec-1, necrostatin-1; OS, overall survival; RT-q, reverse transcription-quantitative; ROS, reactive oxygen species; siRNA, small interfering RNA; TCGA, The Cancer Genome Atlas; VHL, von Hippel-Lindau; xCT, cystine/glutamic acid transporter

Key words: β2-adrenergic receptor, ferroptosis, renal cell carcinoma, sorafenib, stress

Introduction

Kidney cancer accounted for an estimated 434,419 new cases and 155,702 deaths worldwide in 2022 (1). In recent years, advances have been seen in the pharmacotherapy of renal cell carcinoma (RCC), including immune checkpoint inhibitors and molecular targeted drugs (MTDs) (2). Despite these developments, long-term efficacy is observed in ~30% of patients with metastatic RCC, and the remining patients develop resistant to treatment (3-7).

Ferroptosis is a non-apoptotic cell death process in which phospholipids on the cell membrane are converted to lipid peroxide by the oxidant iron and the accumulation of lipid peroxide leads to cell membrane rupture (8,9). Glutathione peroxidase 4 (GPX4) detoxifies lipid peroxides, relying on glutathione (GSH) for its function. The cystine/glutamic acid transporter (xCT) plays a crucial role in maintaining GSH levels. Inhibition of xCT decreases cystine availability,

depleting GSH and leading to GPX4 inactivation, resulting in ferroptosis (10). While sorafenib inhibits xCT and some studies have reported that sorafenib induces ferroptosis (11,12), other reports dispute this claim (13,14). These discrepancies may arise from differences in cell line backgrounds, drug concentration and the ferroptosis markers used to define cell death. Thus, whether sorafenib induces ferroptosis in a cell-type-dependent manner remains unresolved.

Patients with cancer typically experience chronic psychological stress (15), which triggers the secretion of catecholamines, including adrenalin, noradrenalin and dopamine, via the sympathetic nervous system, and cortisol via the hypothalamic-pituitary-adrenal (HPA) axis (16). These stress-induced hormones are implicated in tumor progression and the development of aggressive malignancies (such as ovarian carcinoma) with poor prognosis (16-20). Chronic stress responses, particularly β-adrenergic receptor (ADRB) activation, are associated with cancer progression via activation of signaling pathways such as cAMP-protein kinase, ERK and Akt (19,21). In breast cancer, β-blockers usage is associated with improved prognosis (22-25), while tumors with abundant sympathetic innervation typically exhibit worse outcomes (26). In hepatocellular carcinoma, stimulation of β2-adrenergic receptor (ADRB2) has been reported to contribute to sorafenib resistance (27).

Despite growing evidence from other types of cancer, the role of ADRB2 in RCC remains poorly understood (21,28-30). Xie *et al* (46) demonstrated that ADRB2 undergoes lysosomal degradation mediated by the von Hippel-Lindau (VHL) protein, which is commonly inactivated in clear cell RCC (ccRCC). Secondary analysis using The Cancer Genome Atlas (TCGA) and International Cancer Genome Consortium (ICGC) has shown that lower ADRB2 mRNA expression is associated with higher ccRCC stage and grade, whereas higher ADRB2 expression is associated with better overall survival (OS) (29). In another report, ADRB2 inhibitors demonstrated tumor suppressive effects in $VHL^{-/-}$ RCC cells by upregulating Bax and caspase-3/7, inducing apoptosis, inhibiting angiogenesis via hypoxia-inducible factor (HIF)-2α suppression and reducing inflammation via p65/NF-ϰB inhibition (30). The present study investigated ADRB expression via immunohistochemistry of surgical specimens, as well as ADRB2-mediated stress catecholamine responses and drug resistance in RCC. The present study also explored the role of ferroptosis in sorafenib-induced cytotoxicity against RCC and how ADRB2 stimulation affects ferroptosis.

Materials and methods

Reagents. Medium (RPMI-1640), Lipofectamine 3000, and Lipofectamine RNAiMAX were obtained from Thermo Fisher Scientific, Inc. Fetal bovine serum (FBS) was purchased from AusGeneX. Trypsin-EDTA and isoproterenol (ISO) were obtained from Sigma-Aldrich (Merck KGaA). Sorafenib, cabozantinib, lenvatinib, rapamycin and HIF-2α inhibitor PT2385 were purchased from LC Laboratories. Ferroptosis inhibitor ferrostatin-1 (Fer-1), selective ferroptosis inducer RSL3 and p38 inhibitor SB203580 were purchased from Cayman Chemical Company. Apoptosis inhibitor Z-VAD-FMK (z-VAD), autophagy inhibitor 3-methyladenin (3-MA), necroptosis inhibitor necrostatin-1 (Nec-1), ERK1/2 pathway inhibitor PD0325901 and JNK inhibitor SP600125 were purchased from Adipogen Life Sciences. Ferroptosis inducer erastin was purchased from ChemScene LLC. Propranolol (PRO) hydrochloride was obtained from Sumitomo Pharma.

Cell culture. Human RCC cell lines A-498 (VHL mutant RCC; HIF-1α-negative, HIF-2α-positive), 769-P (VHL mutant RCC; HIF-1α/HIF-2α-negative), 786-O (VHL mutant RCC; HIF-1α negative, HIF-2α-positive), Caki-1 (VHL null RCC; HIF-1α/HIF-2α-negative), Caki-2 (VHL null papillary RCC, HIF-1α/HIF-2α-negative) and ACHN (VHL null RCC, HIF-1α/HIF-2α-negative) were obtained from the American Type Culture Collection. Cells were cultured in RPMI medium supplemented with 50 μg/ml kanamycin and 10% fetal bovine serum in a 5% CO_2, 37˚C incubator. All cell lines were verified to be free of mycoplasma contamination.

Immunohistochemical (IHC) staining. The present study was approved by the Ethics Committee of Yamagata University (Yamagata, Japan; approval no. 2020-425). Written informed consent for the use of clinical samples was obtained from all patients.

The present study investigated the expression of ADRB1 and ADRB2 in primary tumors of 35 patients (26 male and 9 female) diagnosed with metastatic RCC who underwent nephrectomy at Yamagata University Hospital (Yamagata, Japan) between January 2010 and December 2016 using IHC staining. Inclusion criteria were as follows: i) Diagnosis of metastatic disease and ii) age >17 years. Exclusion criteria were: 1) withdrawal of research participation, and 2) insufficient tumor volume of surgical specimen for analysis. Because the number of available cases was limited, no formal statistical power calculation was performed and all samples were included to maximize the descriptive value of the IHC assessment. All IHC staining procedures were conducted in a single batch using identical protocols and reagent lots to minimize technical variability. The median age was 64 (range, 43-77) years. The excised specimens were fixed in 10% formalin at room temperature for 24-48 h and paraffin-embedded. The samples were cut into 3 μm thick sections, placed on Cyanoacrylate®-coated slides (Dako; Agilent Technologies, Inc.) and baked 43˚C for 1 h. Following three 5 min washes with xylene and four 5 min washes with 100% ethanol, paraffin was removed and the samples were dehydrated and hydrated. The samples were subjected to an antigen inactivation procedure at 120˚C for 20 min using 10 mM Tris, 1 mM EDTA (pH 9.0) solution. To inhibit endogenous peroxidase, samples were immersed in 3% hydrogen peroxide-containing methanol solution for 10 min. Rabbit anti-ADRB1 (cat. no. 12271s) and rabbit anti-ADRB2 polyclonal antibody (both 1:50, cat. no. 8513; both Cell Signaling Technology, Inc.) were incubated overnight at 4˚C in a humid environment, then washed with PBS. Sections were treated with HRP-conjugated anti-rabbit IgG (cat. no. P0448, Dako; Agilent Technologies, Inc.; 1:500) for 1 h at room temperature and then washed with PBS. Histofine Simple Stain MAX-PO® (Nichirei Biosciences, Inc.) was incubated for 30 min at room temperature, then the color was developed by reacting with DAB (cat. no. D5905; Sigma-Aldrich; Merck KGaA) for 20 min. Hematoxylin

staining was performed for nuclear staining at room temperature. Immunohistochemical staining for ADRB1 and ADRB2 was evaluated by light microscope using a three-tier scoring system based on staining intensity and the approximate percentage of positive tumor cells. Staining intensity was evaluated by comparing the RCC region with the normal renal tubules on the same histological slide. 'No expression' was defined as absent or trace staining in <5% of tumor cells. 'Low expression' was defined as staining in 5-50% of tumor cells. 'High expression' was defined as staining in >50% of tumor cells. All samples were independently reviewed by two investigators and discrepancies were resolved by consensus.

Reverse transcription-quantitative (RT-q)PCR. RNA was extracted from cells using the Reliaprep RNA Cell Miniprep System (Promega Corporation) and cDNA was synthesized using the High Capacity cDNA RT kit (Applied Biosystems, Thermo Fisher Scientific Inc.), according to the manufacturer's instructions. RT-qPCR was performed using Power Track SYBR Green Master Mix (Thermo Fisher Scientific, Inc.) and CFX Connect Real-Time System (Bio-Rad Laboratories, Inc.). The thermocycling conditions were as follows: Initial denaturation at 95˚C for 2 min, followed by 40 cycles of denaturation at 95˚C for 15 sec and annealing/extension at 60˚C for 1 min. The expression of mRNA was determined using the ΔΔCq method, relative to GAPDH, which was used as an endogenous control (31). The expression levels in each cell line were compared with those in 769P cells. Primers (Integrated DNA Technologies, Inc.) were as follows: ADRB1 forward, 5'-TAC GGCTCCTTCTTCTGCGA-3' and reverse, 5'-TGCATGAGG ATGGGCAGGAA-3'; ADRB2 forward, 5'-ATGGTGTGG ATTGTGTCAGGC-3' and reverse, 5'-TGGAAGCGGCCC TCAGATTT-3' and GAPDH forward, 5'-GCACCGTCAAGG CTGAGAAC-3' and reverse, 5'-TGGTGAAGACGCCAGTGG A-3'.

Western blot analysis. Western blot analysis was performed as previously described (25). Western Blot Hyper HRP Substrate and Western Blot Ultra HRP Substrate® (both Takara Bio, Inc.) were used. Image acquisition was performed with a Light Capture AE-6981 system® and analysis was performed with CS Analyzer ver 3.0 for Windows® (both ATTO Corporation). For the detection of β-receptor proteins, ADRB1 (cat. no. 28323-1-AP; Proteintech Group, Inc.) and ADRB2 (both 1:1,000; 2 h at room temperature; cat. no. 8513; Cell Signaling Technology Japan) antibodies were used. The following antibodies were used to detect intracellular signaling molecules: p38 MAPK (p38; cat. no. 8690), phosphorylated (p-)p38 (T180/Y182; cat. no. 4511), JNK (all 1:1,000 and incubated for 2 h at room temperature; cat. no. 9252), p-JNK (T183/Y185; cat. no. 4668), Erk1/2 (cat. no. 9102), p-Erk1/2 (T202/Y204; cat. no. 4370), Akt (cat. no. 9272) and p-Akt (S473; cat. no. 4060; all Cell Signaling Technology Japan). α-tubulin (all 1:1,000 and incubated for 2 h at room temperature; cat. no. 017-25031) was purchased from FUJIFILM Wako Pure Chemical Corporation. Secondary antibodies were anti-mouse IgG, HRP-conjugated (diluted 1:10,000 and incubated for 1 h at room temperature; cat. no. NA931V, GE Healthcare) and the anti-rabbit IgG, HRP-conjugated (diluted 1:500 and incubated for 1 h at room temperature; cat. no. P0448, Dako; Agilent Technologies, Inc.).

Small interfering (si)RNA. siRNA was used to knockdown ADRB1 and ADRB2. Human-specific siRNA targeting ADRB1 or ADRB2 (10 nM) was transfected using Lipofectamine RNAiMAX. Kanamycin and FBS-free RPMI medium were used during transfection. After 24 at 37˚C, the medium was replaced with RPMI medium containing 10% FBS. Cells were cultured for 24 h at 37˚C before experiments. For ADRB1 knockdown, siADRB1(1) (cat. no. s1118; sense target sequence, 5'-GCUUAUUUAUGUAUCAAUAtt-3'; anti-sense target sequence, 5'-UAUUGAUACAUAAAUAAG Ctg-3'), siADRB1(2) (cat. no. s1119; sense target sequence, 5'-GAAAGACUUGUUUAUAUUAtt-3'; anti-sense target sequence, 5'-UAAUAUAAACAAGUCUUUCta-3') were used. For ADRB2 knockdown, siADRB2(1) (cat. no. s1122; sense target, 5'-CCAGAAGAUUGACAAAUCUtt-3'; anti-sense, 5'-AGAUUUGUCAAUCUUCUGGag-3'), siADRB2(2) (cat. no. s1123; sense, 5'-CUUCUUCAUCGUUAACAUUtt-3', anti-sense, 5'-AAUGUUAACGAUGAAGAAGgg-3') were used. Silencer Negative Control siRNA #1 (cat. no. AM4611; sequence not available) was used as a negative control. ADRB and negative control siRNA were purchased from Thermo Fisher Scientific, Inc.

Cell viability assay. Cell viability was measured using MTS assay. ACHN and A-498 cells were seeded in 96-well plates at a density of 1,000 cells/well and cultured at 37˚C for 24 h. The medium was removed and 100 μl ISO (10 μM) was added to each well. After 24 h, the medium was removed and 100 μl ISO (10 μM) was added to each well., and the cells were cultured for another 24 h at 37˚C. Cell viability was measured using the CellTiter 96 Aqueous One Solution Cell Proliferation Assay (Promega Corporation). Absorbance at 490 nm was measured using an iMark Microplate Reader (Bio-Rad Laboratories, Inc.) as previously described (32).

Cells were pretreated in the presence or absence of 10 μM ISO for 10 min at 37˚C. Subsequently, sorafenib (0.00, 1.25, 2.50, 5.00 or 10.00 μM), cabozantinib (0.00, 1.25, 2.50, 5.00 or 10.00 μM), lenvatinib (0.00, 1.25, 2.50, 5.00, or 10.00 μM), and rapamycin (0.0, 0.1, 1.0, 10.0, or 100.0 nM)was administered to the cells, and the cells were cultured for 48 h at 37˚C.

Cells were pretreated in the presence or absence of 10 μM ISO for 10 min at 37˚C. Subsequently, ACHN cells were treated with erastin (0, 1, 2, 4 or 8 μM) or RSL3 (0, 25, 50, 100, or 200 nM), and cultured for 48 h at 37˚C.

To determine whether ISO acts via ADRB1 or ADRB2 to influence the effect of sorafenib, ACHN cells were treated with siRNA and cultured for 24 h in serum-free medium at 37˚C. The medium was replaced with medium containing 10 μM ISO, 5 μM sorafenib, and 10% FBS. After 24 h at 37˚C, the medium was replaced with medium containing 10 μM ISO, 5 μM sorafenib, and 10% FBS, and the cells were cultured for 24 h at 37˚C.

To investigate whether ADRB inhibitor PRO counteracts the effect of ISO, cell viability was assessed in ACHN cells treated with PRO (0, 1 or 10 μM), sorafenib (0 or 5 μM), and ISO (0 or 10 μM). Sorafenib and PRO were added concurrently with ISO.

To investigate the mechanism underlying sorafenib-induced suppression of cell viability, ACHN and A-498 cells were treated with sorafenib in combination with cell-death inhibitors, including the ferroptosis inhibitor Fer-1 (5 μM), the apoptosis inhibitor z-VAD (20 μM), the autophagy inhibitor 3-MA (20 μM) and the necroptosis inhibitor Nec-1 (20 μM).

cAMP assay. GloSensor cAMP 20F (Promega Corporation) consists of the cAMP-binding domain of protein kinase A and a variant of firefly luciferase. When these components bind cAMP, a structural change occurs that leads to an increase in luminescence (33). ACHN and A-498 cells were transfected with GloSensor cAMP plasmid (100 ng DNA/well) using Lipofectamine 3000 (Invitrogen; Thermo Fisher Scientific, Inc.) at 37˚C. After 24 h transfection, the cells were harvested and incubated with 2 mM endotoxin-free luciferin (Promega Corporation) at 37˚C for 2 h. The cells were then treated with 10 μM ISO. Luciferase luminescence activity was measured using a luminometer (GLOMAX 20/20 LUMINOMETER, Promega Corporation) at baseline and at 1, 3, 5, 10 and 15 min and then every 15 min up to 120 min.

ADRB2 knockdown using short hairpin (sh)RNA. ADRB2 knockdown was performed using a second-generation lentiviral system consisting of pLKO.1-puro, psPAX2, and pVSV-G. Lentiviral particles were generated by transfecting HEK293T cells (kindly provided by Professor Hironobu Asao, Department of Immunology, Yamagata University Faculty of Medicine, Yamagata, Japan) in 6-well plates. For each well, 930 ng of shRNA vector was transfected together with packaging and envelope plasmids at 1:1:1 molar ratio using Lipofectamine 3000 at 37˚C. The culture supernatant containing lentiviral particles was harvested 48 h post-transfection and filtered through a 0.45-μm membrane. ACHN cells were infected with the virus at a multiplicity of infection of 10 for 24 h at 37˚C in the presence of 8 μg/ml polybrene. Cells were selected with puromycin (2 μg/ml) for ~2 weeks before subsequent experiments. The same puromycin concentration was used for both selection and maintenance. The expression of ADRB2 in the infected cells was validated by RT-qPCR and western blotting, as aforementioned. Lentivirus vectors containing the interfering sequence of ADRB2 (shADRB2: SHCLNV MISSION shRNA TRCN0000008085; target sequence, 5'-CCTCAAGACGTTAGGCATCAT-3') and mock (SHC001 MISSION pLKO.1-puro Empty vector control plasmid DNA) was purchased from Sigma-Aldrich (Merck KGaA).

Stressed mouse model and sorafenib administration. All procedures were performed using female BALB/c nude mice (age, 6-7 weeks; weight, 20-25 g; CLEA Japan Inc.) according to the animal welfare regulations of Yamagata University Faculty of Medicine based on the 'Guidelines for the implementation of animal experiments' established by the Ministry of Education, Culture, Sports, Science, and Technology of Japan (34). A total of 20 mice were maintained at 20-26˚C and 40-60% humidity on a 12-h light/dark cycle and were provided with sterilized water and standard rodent feed *ad libitum*, except for stress group during periods of stress induction. All animal studies were approved by the institutional review board of Yamagata University (approval no. R5063, Animal Care and Committee of Yamagata University, Yamagata, Japan).

ACHN cells with ADRB2 knocked down by shRNA ($1x10^7$ cells) were injected with Matrigel (Corning Life Science) into the subcutaneous left flank, while mock-transfected ACHN ($1x10^7$ cells) were injected into the right side. When the tumor volume of negative control ACHN reached ~100 mm^3, the mice were randomly divided into the following groups (all n=5): Control + vehicle, control + sorafenib, stress + vehicle and stress + sorafenib. Blinding was not performed. The mice were housed in metabolic cages for 2 weeks, and then in normal cages for the next 2 weeks. Their urine was collected in a tube containing hydrochloric acid for 3 days (day 10-12) and stored at -80˚C until analysis. The stress groups were placed in a well-ventilated 50 ml conical tube for 6 h/day, as previously described (21). The mice were treated with oral sorafenib (10 mg/kg body weight in saline) or vehicle (saline) once/day. The drug administration and stress induction were conducted 5 days/week for 4 weeks. Tumor growth was measured every 2-3 day and the volume of the xenograft tumors were calculated as length x width x thickness x 0.5. The humane endpoint was tumor volume >1,500 mm^3. However, no mice reached this threshold (maximum volume, 1,487 mm^3). The sample size was calculated on a tumor volume difference of 110 mm^3 between sorafenib-treated stressed and non-stressed mice, with a standard deviation of 60 mm^3, a significance level of 0.05 and a statistical power of 0.8.

After 4 weeks, mice were anesthetized by intraperitoneal administration of medetomidine (0.3 mg/kg), midazolam (4 mg/kg) and butorphanol (5 mg/kg) (35) and euthanized via cervical dislocation. Death was confirmed by the absence of respiration and heartbeat. Blood samples were collected from the inferior vena cava, into EDTA-coated tubes and centrifuged at 2,000 x g for 15 min at 4˚Cto obtain plasma and stored at -80˚C until analysis. The measurement of adrenaline, noradrenaline and dopamine in acidic urine, as well as the measurement of cortisol in plasma, was performed by NIKKEN SEIL Co., Ltd.

Assessment of malondialdehyde (MDA) levels. MDA levels were used to assess the level of ferroptosis. Cells were treated with 10 μM ISO and/or 1 μM erastin at 37˚C for 1 h and collected using a 0.08% Trypsin-0.3 mM EDTA at 37˚C for 2 min. Cell lysate was prepared by sonication for 2 min using 4 cycles of 30 min on and 10 min off, at 20 kHz, while maintained on ice, and MDA concentration was assessed using MDA assay kit (cat. no. M496, Dojindo Laboratories, Inc.) according to the manufacturer's instructions. Fluorescence was measured using a fluorescence plate reader (varioskan LUX, Thermo Fisher Scientific, Inc.).

Reactive oxygen species (ROS) measurement. The present study detected ROS levels to assess the level of ferroptosis. Cells were incubated with RPMI medium containing 5 μM CellRox Deep Red (cat. no. C10422, Thermo Fisher Scientific, Inc.) at 37˚C for 3 h. Next, cells were treated with 10 μM ISO and/or 1 μM erastin at 37˚C for 1 h and collected using 0.08% Trypsin-0.3mM EDTA at 37˚C for 2 min. Following fixation with PBS containing 4% paraformaldehyde at room temperature for 15 min, intracellular ROS levels were assessed

using CellROX Deep Red Reagent (Themo Fisher Scientific),. Fluorescence intensity of the cells was measured using a flow cytometer (FACS Melody, BD Biosciences) and analyzed using FlowJo software version 10.8.1 (BD Biosciences). Each sample was measured in triplicate. The rate of increase in intracellular ROS was calculated as follows: ROS increase %=100 x (fluorescence intensity after treatment-fluorescence intensity of untreated cells)/fluorescence intensity of untreated cells.

Statistical analysis. Comparisons between immunostaining levels and clinical data were performed using cross tabulation and χ^2 or Fisher's exact tests. Kaplan-Meier survival curve analysis and a log-rank test were used to estimate cause-specific survival. Continuous variables are presented as the median or mean ± SD of three independent experimental repeats. Normality was assessed using the Kolmogorov-Smirnov test, and all data sets showed P-values >0.05. Homogeneity of variance was evaluated using the F-test, and all data showed P-values >0.05. Group comparisons of means were analyzed using unpaired t-tests or one- or two-way ANOVA with followed by Dunnett and Bonferroni post hoc tests. P<0.05 was considered to indicate a statistically significant difference. Statistical analyses were performed with GraphPad Prism 9.1.1 software (Dotmatics) and EZR version 1.68 (Saitama Medical Center, Jichi Medical University, Saitama, Japan), which is a graphical user interface for R version 4.5.2 (The R Foundation for Statistical Computing) designed to add statistical functions frequently used in biostatistics (36). Cancer-specific survival (CSS) was defined as the time from the date of diagnosis of metastatic RCC to death from RCC, with censoring at the last follow-up or death from other causes. CSS was estimated using Kaplan-Meier method, and the values were compared using the log-rank test.

Results

ADRB1 and ADRB2 are expressed in RCC surgical tissue. In primary RCC tissue from patients with metastases, expression of both ADRB1 and ADRB2 was confirmed in all cases. Higher ADRB1 expression compared with normal tubules was observed in 29/35 cases (82.9%), while higher ADRB2 expression was detected in 28/35 cases (80.0%). No significant association was found between ADRB expression and clinical factors, including grade, stage and cause-specific survival (Fig. S1A, Table SI).

In ccRCC tissue, there was a mixture of areas that expressed ADRB and areas that did not. No clear association was observed between high-expression regions and specific anatomical locations, such as near the pseudo-capsule, tumor vessels or necrotic areas. In papillary RCC tissue, both ADRB1 and ADRB2 were highly expressed throughout the lesion (Fig. S1B).

Expression of ADRB1 and ADRB2 mRNA and protein in RCC cell lines. mRNA expression levels of ADRB1 and ADRB2 in RCC cell lines were quantified relative to ADRB2 expression in 769-P cells. ADRB1 mRNA levels were comparable among A-498, Caki-1 and Caki-2 but were notably lower in 769-P cells. By contrast, ACHN cells exhibited 11.7-fold higher ADRB1 compared with ADRB2 expression in 769-P cells. ADRB2 mRNA levels were 6.2-fold higher in A-498, 100-fold higher in Caki-1 and 640-fold higher in ACHN than in 769-P cells compared with those in 769P cells (Fig. 1B; Table SII).

Western blot analysis confirmed high protein expression of both ADRB1 and ADRB2 in ACHN cells (Figs. 1C and S2). While ADRB1 was detected in all examined cell lines, ADRB2 expression was minimal except in ACHN cells. Notably, mRNA and protein expression levels were not associated (Figs. 1B and C and S2).

No association was observed between ADRB2 levels and VHL gene mutation in the present study (Figs. 1B and C and S2). Based on these findings, ACHN, a RCC cell line with high ADRB1/2 expression, and A-498, a typical ccRCC cell line with VHL gene mutation, were selected for subsequent experiments.

High-dose ISO attenuates sorafenib-induced suppression of ACHN cell viability. To assess the response of RCC cells to ADRB, cAMP levels were measured in ACHN and A-498 cells following ISO treatment using the GloSensor cAMP 20F. In both cell lines, ISO treatment led to an increase in cAMP levels (Fig. 2A). Viability was evaluated in ACHN and A-498 cells treated with ISO using the MTS assay; however, no significant changes were observed (Fig. 2B). To examine the potential association between ADRB stimulation and drug resistance, an MTS assay was performed in ACHN and A-498 with clinically relevant MTDs, including sorafenib (0-10 μM), cabozantinib (0-20 μM), lenvatinib (0-20 μM) and rapamycin (0-100 nM). The assay was performed under ISO-free conditions and under conditions mimicking physiological ISO concentrations [10 nM (blood levels) and 10 μM (neuronal terminal levels)] (37). Cell viability ratios were calculated relative to MTD-free conditions. No significant difference in cell viability was observed with 10 nM ISO compared with ISO-free conditions for sorafenib treatment. However, at 10 μM ISO, the efficacy of sorafenib was attenuated in ACHN cells. By contrast, in A-498 cells,10 μM ISO did not affect the sorafenib-induced suppression of viability. Additionally, ISO did not influence the drug-induce viability suppression in either ACHN or A-498 cells (Fig. 2C).

To determine whether ADRB1/2 knockdown reverses the attenuation of sorafenib efficacy by ISO, cell viability was assessed in ADRB1/2 knockdown ACHN cells treated with 5 μM sorafenib, in the presence or absence of 10 μM ISO (Figs. 3A and B and S3; Table SIII). While sorafenib treatment decreased cell viability, the addition of ISO attenuated its effect. ADRB2, but not ADRB1, knockdown decreased the attenuating effect of ISO on sorafenib efficacy (Fig. 3C). Furthermore, to explore the potential therapeutic application of ADRB antagonism, cell viability was examined following co-administration of a non-specific ADRB antagonist (PRO). Although 10 μM PRO, which is not clinically achievable, slightly decreased cell viability, low concentrations of PRO did not reverse ISO-induced attenuation of sorafenib efficacy (Fig. 3D).

Restraint stress induces sorafenib resistance in a rodent xenograft model. To investigate the impact of stress-induced catecholamine stimulation on sorafenib resistance and the role of ADRB2 in an *in vivo* model, ADRB2 knockdown ACHN

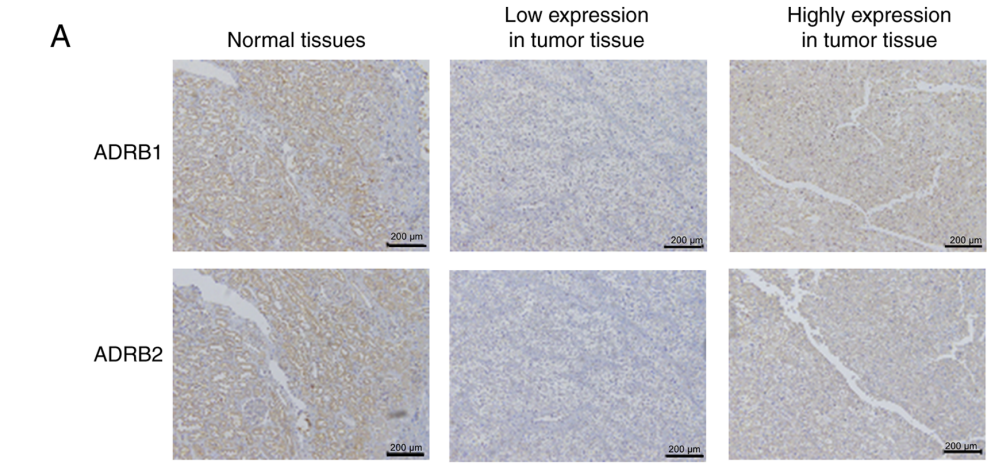

	No expression	Low expression	High expression
ADRB1	0	6 (17.1)	29 (82.9)
ADRB2	0	7 (20.0)	28 (80.0)

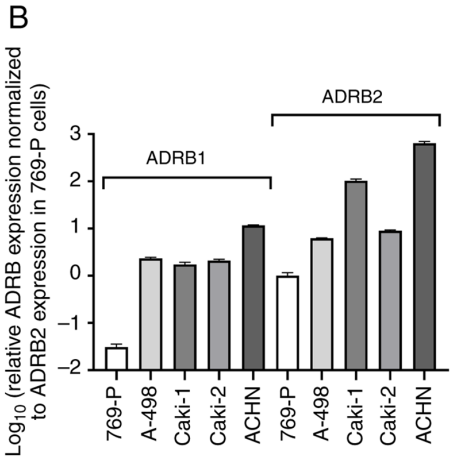

	769-P	A-498	Caki-1	Caki-2	ACHN
VHL mutation	+	+	-	-	-
HIF-1α expression	-	-	-	-	-
HIF-2α expression	+	+	-	-	-
ADRB1	0.03	2.32	1.74	2.10	11.70
ADRB2	1.00	6.20	102.66	8.96	640.29

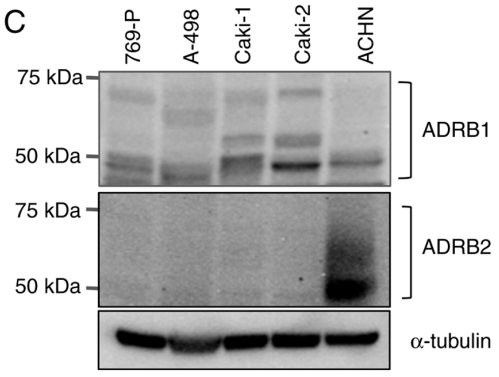

Figure 1. ADRB1/2 expression in RCC. (A) Representative immunohistochemical staining of ADBR1/2 in surgical specimens. A total of >80% of specimens showed high expression of both ADRB1 and ADRB2. Scale bar, 200 μm. (B) ADRB1/2 mRNA expression in RCC cell lines measured by reverse transcription-quantitative PCR. (C) ADRB1/2 protein expression in RCC cell lines measured by western blot analysis. ADRB, β-adrenergic receptor; RCC, renal cell carcinoma; HIF, hypoxia-inducible factor; VHL, von Hippel-Landau.

cells were generated using the shRNA method. ADRB2 mRNA and protein levels decreased in ADRB2 knockdown ACHN cells (Fig. S4A).

Under stress conditions, mice treated with sorafenib exhibited a significant increase in urinary adrenaline and dopamine levels (Fig. 4A), whereas cortisol levels remained unchanged (Fig. 4B).

In control mice inoculated with mock ACHN cells, sorafenib effectively inhibited tumor growth. In the vehicle group, stress exposure did not significantly affect tumor volume. However, in sorafenib-treated mice, the stress group demonstrated a significantly greater increase in tumor volume compared with the control group. By contrast, in mice with

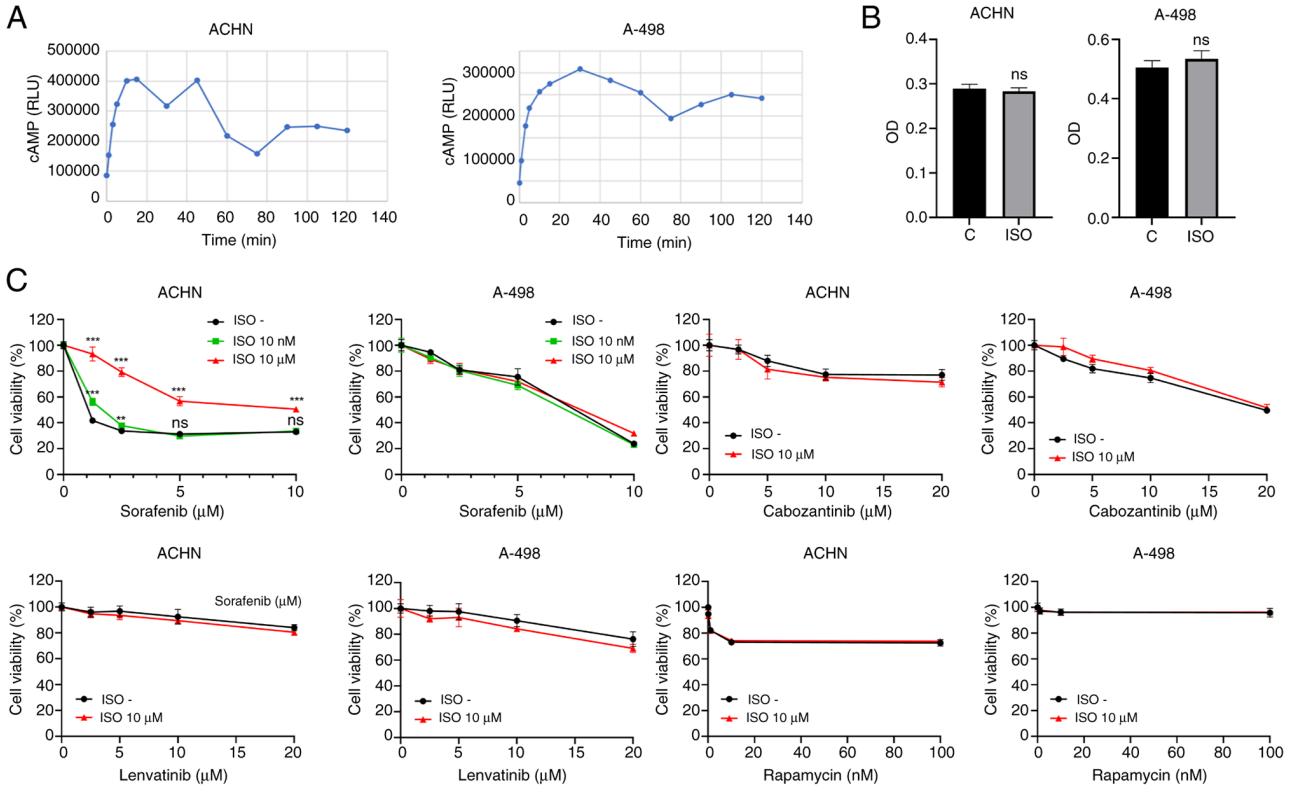

Figure 2. Effect of ADRB on renal cell carcinoma cell lines. (A) cAMP levels after ISO stimulation. (B) Cell viability measured by MTS assay. (C) Cell viability after treatment with sorafenib, cabozantinib, lenvatinib or rapamycin under ISO stimulation. **P<0.01, ***P<0.001 vs. ISO-free control. ADRB, β-adrenergic receptor; ISO, isoproterenol; OD, optical density; n.s., not significant; RLU, relative light unit; C, control.

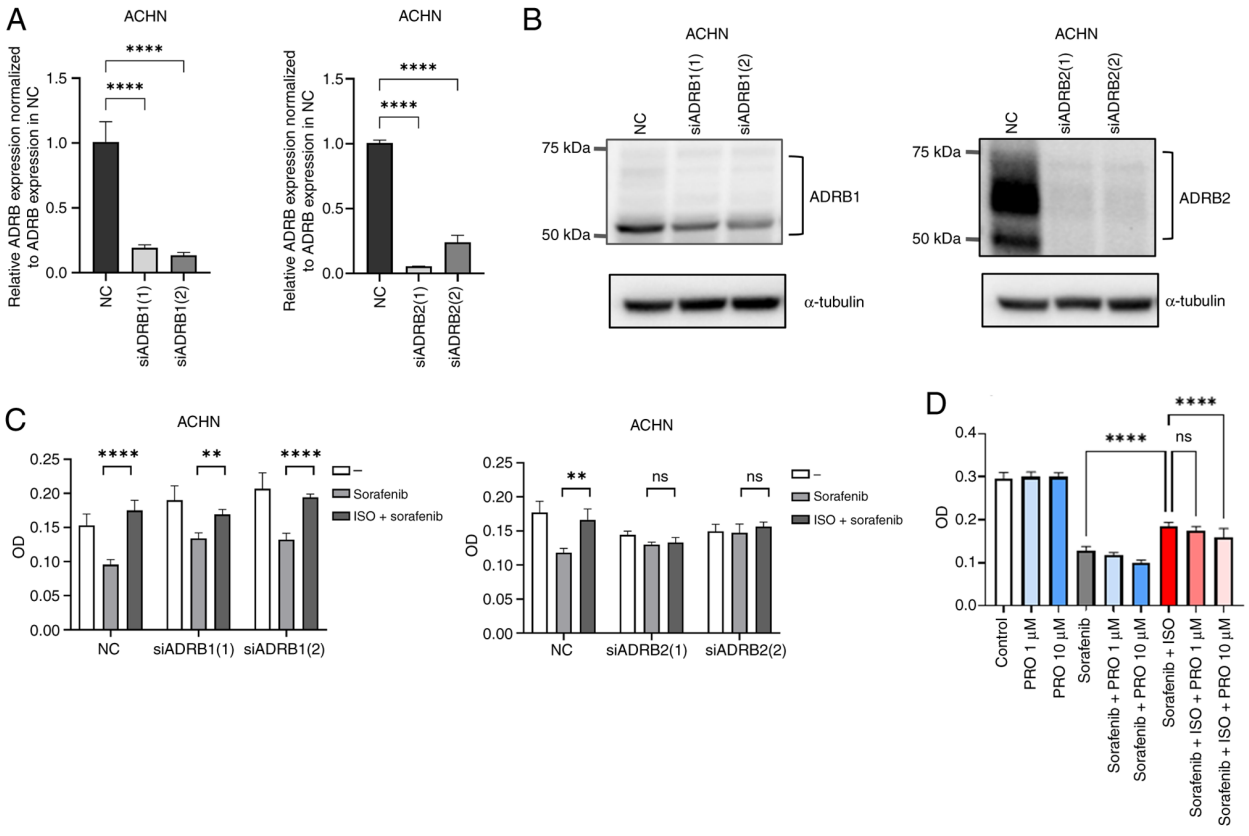

Figure 3. Knockdown or pharmacological inhibition of ADRB1/2.restores sorafenib sensitivity impaired by ISO. ADRB1/2 (A) mRNA. ****P<0.0001 vs. NC. (B) protein expression. (C) Viability of ACHN cells treated with sorafenib or ISO + sorafenib following ADRB1/2 knockdown. **P<0.01; ****P<0.0001 vs. Sorafenib group. (D) Viability of ACHN cells treated with PRO and/or sorafenib and/or ISO. **P<0.01; ****P<0.0001 vs. ISO + sorafenib group. ADRB, β-adrenergic receptor; ISO, isoproterenol; PRO, propranolol; NC, negative control; si, small interfering; OD, optical density; ns, not significant.

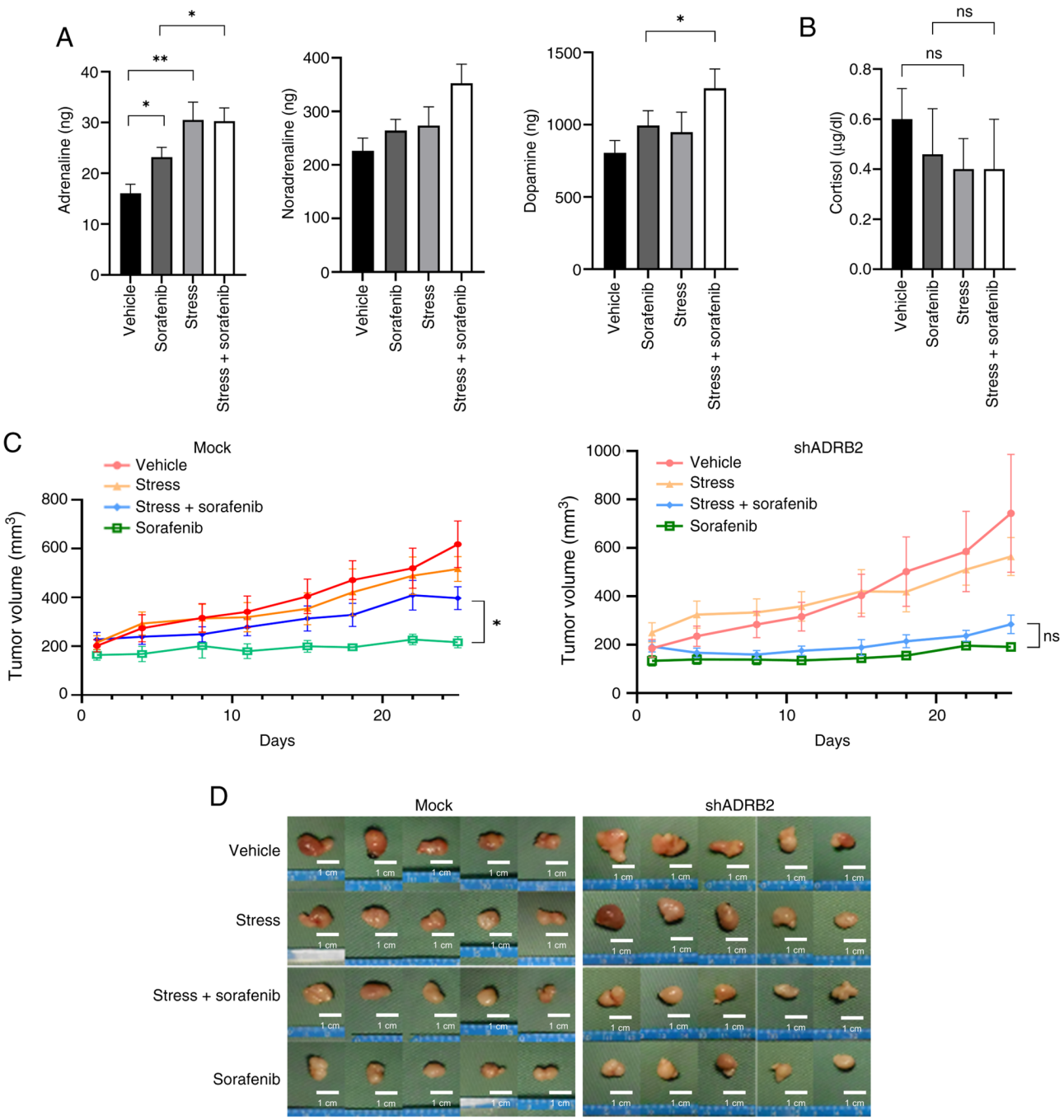

Figure 4. ADRB2 knockdown suppresses restraint stress-induced sorafenib resistance in an ACHN xenograft model. (A) Urine catecholamines (adrenaline, noradrenaline, and dopamine) and (B) serum cortisol levels following sorafenib treatment and/or stress. (C) Tumor volume in (D) mice following sorafenib treatment and/or stress. ADRB, β-adrenergic receptor; sh, short hairpin; ns, not significant; *P<0.05; **P<0.01.

shADRB2 ACHN tumors, no significant differences in tumor volume were observed between the control and stress-exposed groups under sorafenib treatment, with both groups showing suppressed tumor growth (Fig. 4C and D). These findings suggested that stress-induced ADRB2 activation attenuated the anti-tumor effect of sorafenib.

ISO mitigates ferroptosis induced by sorafenib, erastin and RSL3. To investigate the mechanisms underlying sorafenib-induced suppression of cell viability, the present study assessed its effects using the ferroptosis inhibitor Fer-1, the apoptosis inhibitor z-VAD, the autophagy inhibitor 3-MA and the necroptosis inhibitor Nec-1. In ACHN cells, Fer-1 counteracted the decrease in cell viability caused by sorafenib, whereas z-VAD, 3-MA and Nec-1 had no impact on sorafenib-induced suppression of cell viability (Fig. 5A). These findings suggested that sorafenib decreased viability in ACHN cells via ferroptosis induction. However, in A498 cells, Fer-1 did not reverse sorafenib-induced suppression of cell viability, indicating that sorafenib-induced ferroptosis exhibited cell line-dependent variability.

The present study examined the effects of ISO on ferroptosis inducers erastin and RSL3. Although these inducers decreased cell viability, ISO mitigated their effects (Fig. 5B).

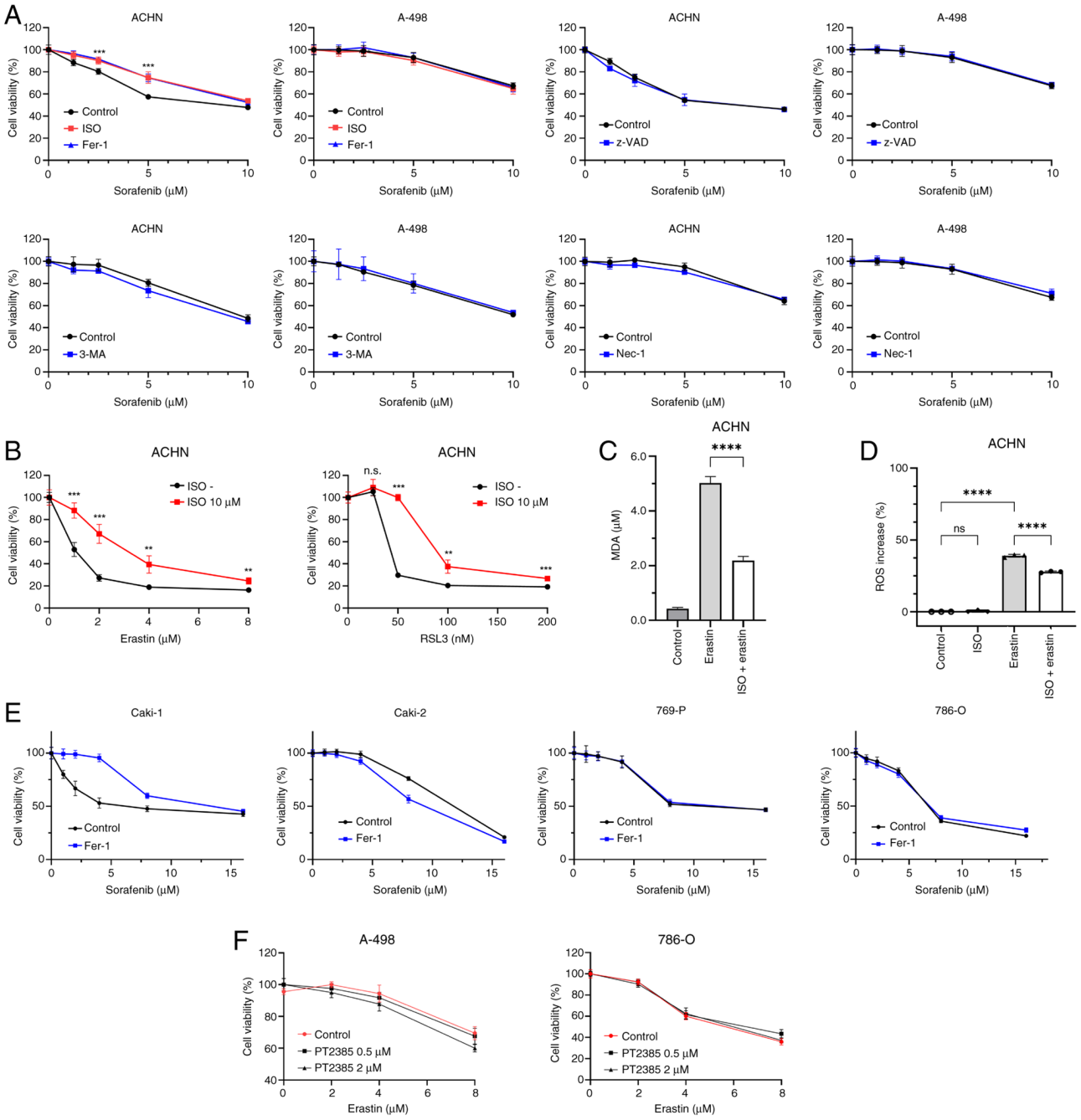

Figure 5. ISO mitigates ferroptosis induced by sorafenib, erastin and RSL3. (A) Viability of ACHN or A498 cells treated with sorafenib and ferroptosis inhibitor Fer-1, apoptosis inhibitor z-VAD, the autophagy inhibitor 3-MA and the necroptosis inhibitor Nec-1. (B) Viability of ACHN cells treated with ISO and erastin or RSL3. (C) MDA and (D) ROS levels in cells treated by erastin ± ISO. (E) Viability of Caki-1, Caki-2, 769P and 786-O cells treated with sorafenib and Fer-1. (F) Viability of A-498 and 786-O cells treated with erastin and PT2385. ISO, isoproterenol; MDA, malondialdehyde; ROS, reactive oxygen species; ns, not significant; Fer -1, ferrostatin-1; z-VAD, Z-VAD-FMK; 3-MA, 3-methyladenin; Nec-1, necrostatin-1. **P<0.01; ***P<0.001; ****P<0.0001.

Additionally, erastin increased levels of the lipid peroxidation marker MDA but this increase was inhibited by ISO (Fig. 5C). Similarly, erastin treatment led to increased ROS levels, which were suppressed by ISO (Fig. 5D). These results indicated that ISO suppressed ferroptosis induced by erastin and RSL3.

Sorafenib induces ferroptosis in ACHN and Caki-1, but not in A498, Caki-2, 769P and 786-O cells. The present study investigated sorafenib-induced ferroptosis in additional RCC cell lines, including Caki-1, Caki-2, 769-P and 786-O. Fer-1 rescued sorafenib-induced loss of viability in Caki-1 cells, but had no protective effect in Caki-2, 769-P and 786-O cells (Fig. 5E). Sorafenib did not decrease cell viability at clinically achievable concentrations (<5 μM). Because VHL-mutant cell lines did not exhibit sorafenib-induced ferroptosis and loss of VHL leads to stabilization of HIF-2α (38), the present study examined whether ferroptosis susceptibility was influenced by HIF-2α, the key oncogenic driver in ccRCC. In HIF-2α-positive, VHL mutant A-498 and 786-O cells, HIF2α inhibitor PT2385 failed to reverse erastin-indued loss of viability, indicating that HIF-2α did not modulate ferroptosis under these conditions (Fig. 5F).

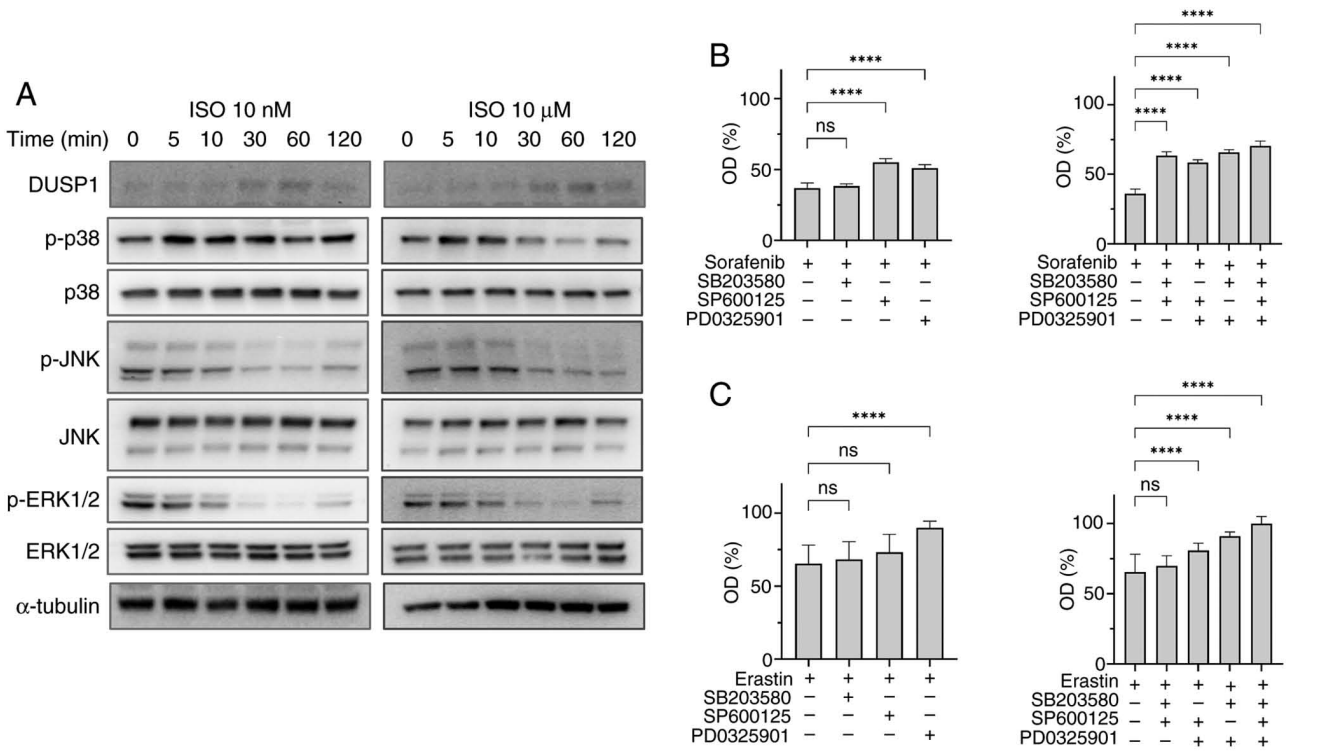

Figure 6. ISO upregulates DUSP1 and suppresses MAPK phosphorylation, which mitigates the effect of sorafenib and erastin. (A) Levels of DUSP1 and MAPK phosphorylation following treatment with ISO. (B) Viability of ACHN cells treated by sorafenib and/or MAPK inhibitors, including p38 inhibitor SB203580, JNK inhibitor SP600125 and ERK1/2 inhibitor PD0325901. (C) Viability of ACHN cells treated with erastin and/or MAPK inhibitors, ISO, isoproterenol; DUSP1, dual-specific phosphatase 1; p-, phosphorylated; ns, not significant; OD, optical density. ****P<0.0001.

ISO-induced ferroptosis resistance is mediated by MAPK pathway attenuation. A previous study demonstrated that adrenaline increases dual-specificity phosphatase 1 (DUSP1) expression, which inhibits the phosphorylation of MAPKs (39). Additionally, multiple studies have shown that MAPK, ERK1/2, p38, and JNK pathways enhance ferroptosis induction (12,40,41). To investigate the mechanisms by which ISO modulates ferroptosis, the present study assessed the effect of ISO on DUSP1 expression and MAPK phosphorylation. ISO upregulated DUSP1. Phosphorylation of JNK and ERK was inhibited by both 10 nM and 10 μM ISO, whereas inhibition of p38 phosphorylation was observed only at the higher concentration (Figs. 6A and S5A). The present study assessed cell viability following treatment with ferroptosis inducers and MAPK inhibitors. The JNK inhibitor SP600125 and ERK1/2 inhibitor PD0325901 attenuated the effects of sorafenib and erastin. Moreover, simultaneous inhibition ERK1/2, p38 or JNK suppressed ferroptosis induction (Figs. 6B and C and S5B and C).

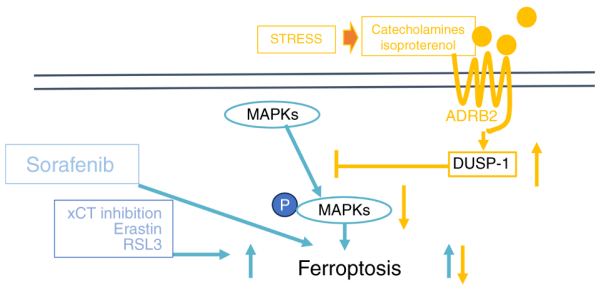

Figure 7. Sorafenib induces ferroptosis in ACHN cells, and this effect is attenuated by ADRB2 stimulation. DUSP1, dual-specific phosphatase 1; xCT, cystine/glutamic acid transporter; ADRB2, β2-adrenergic receptor.

Discussion

The present study demonstrated that ADRB2 was expressed in RCC cells and its activation mitigated sorafenib-induced ferroptosis both *in vitro* and *in vivo* (Fig. 7). ADRB1/2 proteins were detected in all RCC specimens. Previous studies have reported that ferroptosis-associated pathways influence therapeutic response and prognosis in RCC (42,43). By contrast, transcriptomic data from TCGA and ICGC indicate that higher ADRB2 mRNA expression is associated with lower stage and improved OS (29), and the present findings did not establish an association between ADRB2 protein expression and clinical factors. This suggests that ADRB2 does not function as a determinant of tumor aggressiveness but exerts biological effects in a context-dependent manner. Specifically, ADRB2-mediated signaling may modulate ferroptosis and therapeutic response under pharmacological stress or enhanced adrenergic stimulation, rather than influencing baseline tumor behavior. Accordingly, ADRB2 protein expression alone is unlikely to serve as a robust prognostic biomarker in RCC but may influence treatment response only under specific conditions such as ferroptosis-inducing or adrenergic stress environments. Additionally, the difference in mRNA and protein expression may stem from lack of association between protein and mRNA expression levels in G protein-coupled receptors (44,45), a trend consistent

with the present findings that ADRB1/2 mRNA and protein levels discordant. A previous study reported that VHL protein promotes ADRB2 degradation, leading to ADRB2 accumulation in ccRCC, which harbors VHL gene inactivation (46). However, in the present study, ADRB2 protein expression was not associated with VHL gene mutation. In most clinical samples, there were regions where ADRB2 was expressed and others where it was not, suggesting an unidentified mechanism regulating ADRB2 expression that warrants further investigation.

Chronic stress negatively influence cancer progression (15,21), primarily via catecholamine-mediated mechanisms (17-19). Here, ISO alone did not affect cell viability, either *in vitro* or in the mouse model. Furthermore, the expression levels of ADRB2 in patient tumor tissue were not significantly associated with clinicopathological parameters, including tumor grade, stage or cause-specific survival. These findings indicate that stress-induced ADRB stimulation by ISO alone is insufficient to directly influence RCC cell survival or clinical prognosis.

ISO suppressed the anti-tumor effect of sorafenib in ACHN cells, an ADRB2-expressing cell line. This ISO-induced suppression was inhibited by high doses of PRO and ADRB2 knockdown. These findings suggest that ADRB2 activation underlies this phenomenon, however, clinically relevant doses of PRO failed to restore the sorafenib effect. Additionally, ISO-induced suppression required high-dose ISO, consistent with concentrations in nerve terminals (37). A prior study reported that PRO alone suppresses RCC cell viability (30), yet the present findings did not corroborate this effect. Plasma catecholamine concentrations in humans are typically in the low nanomolar range, however, neurotransmitter release from sympathetic nerve terminals generates transient micromolar concentrations within the synaptic cleft, which are not reflected by circulating levels (37). Thus, the supraphysiological ISO concentrations used *in vitro* may model intense, localized adrenergic signaling rather than systemic exposure. Nevertheless, use of supraphysiological ISO concentrations limit direct clinical translation, as *in vitro* ISO exposure does not recapitulate the spatially restricted nature of adrenergic neurotransmission *in vivo*.

Complete pharmacological suppression of high-intensity adrenergic signaling at sympathetic nerve terminals is unlikely to be clinically feasible. Although PRO accumulates within lipid-rich neural membranes and may reach low micromolar concentrations (~5 μM) at nerve terminals (47), the present data indicate that 10 μM PRO (a concentration exceeding estimated physiological tissue levels) did not significantly attenuate ISO-mediated suppression of sorafenib efficacy. This suggested that localized catecholamine surges within the synaptic cleft may exceed the antagonistic capacity of clinically tolerable β-blocker exposure. Achieving sufficient ADRB2 antagonism to counteract transient micromolar catecholamine surges may compromise essential sympathetic functions, including vascular tone and blood pressure regulation, and therefore may not be physiologically tolerable. Consequently, clinically achievable ADRB blocker dosing is unlikely to fully antagonize localized nerve terminal-derived catecholamine signaling within the tumor microenvironment. The clinical relevance of ADRB modulation thus remains uncertain, particularly with respect to PRO dosing, tissue-level receptor occupancy and the disparity between local and circulating catecholamine concentrations.

Recent studies have suggested that ferroptosis enhances antitumor immunity and improves the efficacy of immune checkpoint inhibitors (48-50). The present findings suggest that therapeutic strategies combining stress reduction, ferroptosis-inducing agents such as sorafenib and immune checkpoint blockade may represent a promising approach for RCC. Although the present data established a mechanistic role for ADRB2 signaling in ferroptosis resistance, further *in vivo* and clinical studies are required to determine whether modulation of adrenergic stress response, pharmacologically or behaviorally, augments ferroptosis-based therapies and immunotherapy in patients.

Albiñana *et al* (30) demonstrated that adding PRO or an ADRB2 inhibitor to 786O cells decreases ROS levels by enhancing the activity of enzymes involved in ROS metabolism, particularly glutathione peroxidase. While this may seem contradictory to the present observation that ADRB2 activation attenuates ferroptosis, this is not inconsistent with the aforementioned study, which was performed in a GSH-replete environment, while ferroptosis induction in the present study occurred under GSH-depleted conditions caused by sorafenib, erastin or RSL3. xCT inhibition by sorafenib, erastin or RSL3 suppresses GSH synthesis, a key factor in mitigating ROS-induced damage. Furthermore, ROS plays a complex role in cell processes, with high ROS levels triggering ferroptosis-induced cell death in tumor cells, as observed in the present study, whereas moderate ROS levels have been reported to promote tumor proliferation and activate pro-survival signaling pathways (51).

The present study into the inhibitory effect of ISO on ferroptosis revealed the involvement of MAPKs in ferroptotic regulation, consistent with prior research (41). Previous studies have shown that adrenaline increases DUSP1, thereby inhibiting MAPK phosphorylation (39,52). Additionally, noradrenaline-induced DUSP1 expression is mediated by the activation of the cAMP/PLC/PKC/CREB signaling pathway via ADRB2, which inhibits JNK-mediated c-Jun phosphorylation and protects ovarian cancer cells from apoptosis (53). Here, ISO upregulated DUSP1 expression and high concentration of ISO suppressed MAPK phosphorylation, thereby inhibiting ferroptosis.

Currently, immune checkpoint inhibitors and MTDs targeting vascular endothelial growth factor receptor (VEGFR) constitute the primary therapeutic approaches for RCC, while agents with direct cytotoxic effects remain limited and typically exhibit insufficient efficacy (7). Sorafenib, an MTD that targets multiple kinases, including VEGFR family, platelet-derived growth factor receptor family, c-kit, raf, p38, feline McDonough sarcoma virus-like tyrosine kinase 3 and xCT, was historically used for RCC treatment (11) but is no longer prioritized in contemporary clinical practice, as per current clinical guidelines (54,55). Although sorafenib has been reported to induce ferroptosis via xCT inhibition (56,57), findings regarding its cytotoxic effects remain inconclusive (13). The present findings revealed that sorafenib induced ferroptosis in ACHN and Caki-1 cells, but not in other cells, highlighting cell line-dependent variability in ferroptosis

sensitivity. Cell lines that exhibited ferroptosis by induced sorafenib exhibited direct sensitivity to clinically available concentration of sorafenib (58). These findings suggested that ferroptosis contributed to sorafenib-induced cytotoxicity only in cell lines that exhibit direct sensitivity to sorafenib, such as ACHN and Caki-1 cells. This variability may contribute to the mixed clinical responses to sorafenib, with certain RCC tumors undergoing sorafenib-induced ferroptosis, while others remain resistant. The mechanism by which sorafenib induces ferroptosis may vary among cell lines and remains unresolved, posing a challenge for future research. Additionally, although A498, 769-P and 786-O cells harbor VHL alterations, sorafenib-induced ferroptosis was not observed in these cell lines. Because VHL loss leads to stabilization and accumulation of HIF-2α, the key oncogenic driver in RCC, the present study examined whether HIF-2α contributes to ferroptosis susceptibility (59). However, pharmacological inhibition of HIF-2α did not influence ferroptosis. Moreover, ferroptosis was not induced in VHL-wild-type Caki-2 cells, indicating that neither VHL status nor HIF-2α activity fully accounts for the differential ferroptotic response to sorafenib. These findings suggest that sorafenib-induced ferroptosis is cell type-specific and may depend on additional molecular or metabolic determinants beyond VHL status. Further studies are needed to identify predictive biomarkers for sorafenib responsiveness and provide novel strategies to overcome therapeutic resistance.

Another limitation of the present study is the use of a restraint model for stress induction in mice, which may introduce confounding factors beyond catecholamine-mediated effects. Although restraint stress activates multiple physiological systems, including the HPA axis and immune responses, it is also a well-established model for robust activation of the sympathetic nervous system and subsequent catecholamine release (21,60). In the present study, urine corticosterone levels did not show a significant difference between stressed and control mice, suggesting that activation of the HPA axis was not a dominant contributor. This supports the hypothesis that sympathetic adrenergic signaling, rather than glucocorticoid-mediated effects, serves a primary role in the stress-associated modulation of sorafenib responsiveness *in vivo*. Furthermore, the present study demonstrated that genetic knockdown of ADRB2 abrogated the stress-mimicking effects of adrenergic stimulation on sorafenib sensitivity *in vitro*, providing direct mechanistic evidence that ADRB2-dependent signaling mediated the observed phenotype. Together with the *in vivo* stress data, these findings support a model in which activation of the sympathetic nervous system modulates therapeutic responses via tumor-intrinsic adrenergic signaling pathways. Nevertheless, restraint stress represents an acute physical stress paradigm and does not fully recapitulate chronic psychological stress encountered in clinical settings. Physical discomfort or systemic inflammation cannot be fully excluded, and because multiple stress-responsive pathways may be simultaneously engaged, the observed effects cannot be attributed exclusively to sympathetic signaling. Further studies may benefit from more selective interventions, such as pharmacological sympathetic blockade, adrenalectomy or comprehensive catecholamine profiling. Although these methods involve technical and physiological complexity, they represent important avenues for clarifying the upstream regulatory architecture of this response.

Lastly, the relatively small clinical and animal sample sizes represent a limitation of this study; studies with larger, independently replicated cohort are required to validate the present findings.

In conclusion, ADRB2attenuates ferroptosis. ADRB2 activation during chronic stress compromises sorafenib efficacy by suppressing ferroptosis in RCC.

Acknowledgements

Not applicable.

Funding

The present study was supported by Grants-in-Aid for Scientific Research (grant nos. JP20K18085 and JP23K15777).

Availability of data and materials

The data generated in the present study may be requested from the corresponding author.

Authors' contributions

MU analyzed data, performed experiments and wrote the manuscript. SN conceived and designed the study and edited the manuscript. HI designed and performed experiments and analyzed data. YT, YO, MY, TN and HF conceived and designed the study and performed experiments. NT, HK, HN and OI conceived and designed the study. MU, SN and NT confirm the authenticity of all the raw data. All authors have read and approved the final manuscript.

Ethics approval and consent to participate

The present study was approved by the Ethics Committee of Yamagata University (Yamagata, Japan) based on the Declaration of Helsinki (approval no. 2020-425). Written informed consent for the use of clinical samples was obtained from all patients. Animal experiments were approved by the Institutional Animal Care and Use Committee of Yamagata University (approval no. R5063).

Patient consent for publication

Not applicable.

Competing interests

The authors declare that they have no competing interests.

Use of artificial intelligence tools

During the preparation of this work, artificial intelligence tools were used to improve the readability and language of the manuscript, and subsequently, the authors revised and edited the content produced by the artificial intelligence tools as

necessary, taking full responsibility for the ultimate content of the present manuscript.

References

1. Bray F, Laversanne M, Sung H, Ferlay J, Siegel RL, Soerjomataram I and Jemal A: Global cancer statistics 2022: GLOBOCAN estimates of incidence and mortality worldwide for 36 cancers in 185 countries. CA Cancer J Clin 74: 229-263, 2024.
2. Rose TL and Kim WY: Renal cell carcinoma: A review. JAMA 332: 1001-1010, 2024.
3. Tannir NM, Albigès L, McDermott DF, Burotto M, Choueiri TK, Hammers HJ, Barthélémy P, Plimack ER, Porta C, George S, *et al*: Nivolumab plus ipilimumab versus sunitinib for first-line treatment of advanced renal cell carcinoma: extended 8-year follow-up results of efficacy and safety from the phase III CheckMate 214 trial. Ann Oncol 35: 1026-1038, 2024.
4. Motzer RJ, Porta C, Eto M, Powles T, Grünwald V, Hutson TE, Alekseev B, Rha SY, Merchan J, Goh JC, *et al*: Lenvatinib plus pembrolizumab versus sunitinib in first-line treatment of advanced renal cell carcinoma: Final prespecified overall survival analysis of CLEAR, a phase III study. J Clin Oncol 42: 1222-1228, 2024.
5. Powles T, Burotto M, Escudier B, Apolo AB, Bourlon MT, Shah AY, Suárez C, Porta C, Barrios CH, Richardet M, *et al*: Nivolumab plus cabozantinib versus sunitinib for first-line treatment of advanced renal cell carcinoma: Extended follow-up from the phase III randomised CheckMate 9ER trial. ESMO open 9: 102994, 2024.
6. Plimack ER, Powles T, Stus V, Gafanov R, Nosov D, Waddell T, Alekseev B, Pouliot F, Melichar B, Soulières D, *et al*: Pembrolizumab plus axitinib versus sunitinib as first-line treatment of advanced renal cell carcinoma: 43-month follow-up of the phase 3 KEYNOTE-426 study. Eur Urol 84: 449-454, 2023.
7. Yochum ZA and Braun DA: Immunotherapy for renal cell carcinoma-what more is to come? Target Oncol 20: 467-483, 2025.
8. Dixon SJ, Lemberg KM, Lamprecht MR, Skouta R, Zaitsev EM, Gleason CE, Patel DN, Bauer AJ, Cantley AM, Yang WS, *et al*: Ferroptosis: An iron-dependent form of nonapoptotic cell death. Cell 149: 1060-1072, 2012.
9. Yang WS, SriRamaratnam R, Welsch ME, Shimada K, Skouta R, Viswanathan VS, Cheah JH, Clemons PA, Shamji AF, Clish CB, *et al*: Regulation of ferroptotic cancer cell death by GPX4. Cell 156: 317-331, 2014.
10. Stockwell BR, Friedmann Angeli JP, Bayir H, Bush AI, Conrad M, Dixon SJ, Fulda S, Gascón S, Hatzios SK, Kagan VE, *et al*: Ferroptosis: A regulated cell death nexus linking metabolism, redox biology, and disease. Cell 171: 273-285, 2017.
11. Yousef EH, El Gayar AM and El-Magd NFA: Insights into Sorafenib resistance in hepatocellular carcinoma: Mechanisms and therapeutic aspects. Crit Rev Oncol Hematol 212: 104765, 2025.
12. Song Q, Peng S, Che F and Zhu X: Artesunate induces ferroptosis via modulation of p38 and ERK signaling pathway in glioblastoma cells. J Pharmacol Sci 148: 300-306, 2022.
13. Zheng J, Sato M, Mishima E, Sato H, Proneth B and Conrad M: Sorafenib fails to trigger ferroptosis across a wide range of cancer cell lines. Cell Death Dis 12: 698, 2021.
14. Guo L, Hu C, Yao M and Han G: Mechanism of sorafenib resistance associated with ferroptosis in HCC. Front Pharmacol 14: 1207496, 2023.
15. Thekdi SM, Milbury K, Spelman A, Wei Q, Wood C, Matin SF, Tannir N, Jonasch E, Pisters L and Cohen L: Posttraumatic stress and depressive symptoms in renal cell carcinoma: Association with quality of life and utility of single-item distress screening. Psychooncology 24: 1477-1484, 2015.
16. Dai S, Mo Y, Wang Y, Xiang B, Liao Q, Zhou M, Li X, Li Y, Xiong W, Li G, *et al*: Chronic stress promotes cancer development. Front Oncol 10: 1492, 2020.
17. Lutgendorf SK, Degeest K, Dahmoush L, Farley D, Penedo F, Bender D, Goodheart M, Buekers TE, Mendez L, Krueger G, *et al*: Social isolation is associated with elevated tumor norepinephrine in ovarian carcinoma patients. Brain Behav Immun 25: 250-255, 2011.
18. Pu J, Zhang X, Luo H, Xu L, Lu X and Lu J: Adrenaline promotes epithelial-to-mesenchymal transition via HuR-TGFβ regulatory axis in pancreatic cancer cells and the implication in cancer prognosis. Biochem Biophys Res Commun 493: 1273-1279, 2017.
19. Zhang X, Zhang Y, He Z, Yin K, Li B, Zhang L and Xu Z: Chronic stress promotes gastric cancer progression and metastasis: An essential role for ADRB2. Cell Death Dis 10: 788, 2019.
20. Yang H, Xia L, Chen J, Zhang S, Martin V, Li Q, Lin S, Chen J, Calmette J, Lu M, *et al*: Stress-glucocorticoid-TSC22D3 axis compromises therapy-induced antitumor immunity. Nat Med 25: 1428-1441, 2019.
21. Thaker PH, Han LY, Kamat AA, Arevalo JM, Takahashi R, Lu C, Jennings NB, Armaiz-Pena G, Bankson JA, Ravoori M, *et al*: Chronic stress promotes tumor growth and angiogenesis in a mouse model of ovarian carcinoma. Nat Med 12: 939-944, 2006.
22. Barron TI, Connolly RM, Sharp L, Bennett K and Visvanathan K: Beta blockers and breast cancer mortality: A population-based study. J Clin Oncol 29: 2635-2644, 2011.
23. Melhem-Bertrandt A, Chavez-Macgregor M, Lei X, Brown EN, Lee RT, Meric-Bernstam F, Sood AK, Conzen SD, Hortobagyi GN and Gonzalez-Angulo AM: Beta-Blocker use is associated with improved relapse-free survival in patients with triple-negative breast cancer. J Clin Oncol 29: 2645-2652, 2011.
24. Cardwell CR, Coleman HG, Murray LJ, Entschladen F and Powe DG: Beta-blocker usage and breast cancer survival: A nested case-control study within a UK clinical practice research datalink cohort. Int J Epidemiol 42: 1852-1861, 2013.
25. Shaashua L, Shabat-Simon M, Haldar R, Matzner P, Zmora O, Shabtai M, Sharon E, Allweis T, Barshack I, Hayman L, *et al*: Perioperative COX-2 and β-Adrenergic blockade improves metastatic biomarkers in breast cancer patients in a phase-II Randomized trial. Clin Cancer Res 23: 4651-4661, 2017.
26. Kamiya A, Hayama Y, Kato S, Shimomura A, Shimomura T, Irie K, Kaneko R, Yanagawa Y, Kobayashi K and Ochiya T: Genetic manipulation of autonomic nerve fiber innervation and activity and its effect on breast cancer progression. Nat Neurosci 22: 1289-1305, 2019.
27. Wu FQ, Fang T, Yu LX, Lv GS, Lv HW, Liang D, Li T, Wang CZ, Tan YX, Ding J, *et al*: ADRB2 signaling promotes HCC progression and sorafenib resistance by inhibiting autophagic degradation of HIF1α. J Hepatol 65: 314-324, 2016.
28. Sato Y, Yoshizato T, Shiraishi Y, Maekawa S, Okuno Y, Kamura T, Shimamura T, Sato-Otsubo A, Nagae G, Suzuki H, *et al*: Integrated molecular analysis of clear-cell renal cell carcinoma. Nat Genet 45: 860-867, 2013.
29. Ha M, Kim DW, Kim J, Hong CM, Park SM, Woo IA, Kim MY, Koo H, Namkoong J, Kim J, *et al*: Prognostic role of the beta-2 adrenergic receptor in clear cell renal cell carcinoma. Anim Cells Syst (Seoul) 23: 365-369, 2019.
30. Albiñana V, Gallardo-Vara E, De Rojas-P I, Recio-Poveda L, Aguado T, Canto-Cano A, Aguirre DT, Serra MM, González-Peramato P, Martínez-Piñeiro L, *et al*: Targeting β2-Adrenergic receptors shows therapeutical benefits in clear cell renal cell carcinoma from von hippel-lindau disease. J Clin Med 9: 2740, 2020.
31. Livak KJ and Schmittgen TD: Analysis of relative gene expression data using real-time quantitative PCR and the 2(-Delta Delta C(T)) Method. Methods 25: 402-408, 2001.
32. Ito H, Ichiyanagi O, Naito S, Bilim VN, Tomita Y, Kato T, Nagaoka A and Tsuchiya N: GSK-3 directly regulates phospho-4EBP1 in renal cell carcinoma cell-line: An intrinsic subcellular mechanism for resistance to mTORC1 inhibition. BMC Cancer 16: 393, 2016.
33. Obara Y, Yanagihata Y, Abe T, Dafik L, Ishii K and Nakahata N: Gα(h)/transglutaminase-2 activity is required for maximal activation of adenylylcyclase 8 in human and rat glioma cells. Cell Signal 25: 589-597, 2013.
34. The Ministry of Education, Culture, Sports, Science, and Technology of Japan: Guidelines for the implementation of animal experiments (In Chinese). https://www.mext.go.jp/b_menu/hakusho/nc/06060904.htm.
35. Leon C, Ruelle A, Geoffray J, Augeul L, Vogt C, Chiari P, Gomez L, Ovize M, Bidaux G and Pillot B: Evaluation of general anesthesia protocols for a highly controlled cardiac ischemia-reperfusion model in mice. PLoS One 19: e0309799, 2024.
36. Kanda Y: Investigation of the freely available easy-to-use software 'EZR' for medical statistics. Bone Marrow Transplant 48: 452-458, 2013.
37. Bell C and Vogt M: Release of endogenous noradrenaline from an isolated muscular artery. J Physiol 215: 509-520, 1971.
38. Kondo K, Klco J, Nakamura E, Lechpammer M and Kaelin WG Jr: Inhibition of HIF is necessary for tumor suppression by the von Hippel-Lindau protein. Cancer Cell 1: 237-246, 2002.

39. Shubin NJ, Pham TN, Staudenmayer KL, Parent BA, Qiu Q and O'Keefe GE: A potential mechanism for immune suppression by beta-adrenergic receptor stimulation following traumatic injury. J Innate Immun 10: 202-214, 2018.
40. Guo M, Huang X, Zhang J, Huang Y, Tang Y, Wen H, Xu Y, Zhang S, Wei X, Sun S and Zhu Q: Palmitic acid induces β-cell ferroptosis by activating ceramide signaling pathway. Exp Cell Res 440: 114134, 2024.
41. Wang X, Tan X, Zhang J, Wu J and Shi H: The emerging roles of MAPK-AMPK in ferroptosis regulatory network. Cell Commun Signal 21: 200, 2023.
42. Xu F, Guan Y, Xue L, Zhang P, Li M, Gao M and Chong T: The roles of ferroptosis regulatory gene SLC7A11 in renal cell carcinoma: A multi-omics study. Cancer Med 10: 9078-9096, 2021.
43. Ren Z, Zhang X and Han J: Expression and prognostic significance of ferroptosis-related proteins SLC7A11 and GPX4 in renal cell carcinoma. Protein Pept Lett 30: 868-876, 2023.
44. Heydenreich FM, Vuckovic Z, Matkovic M and Veprintsev DB: Stabilization of G protein-coupled receptors by point mutations. Front Pharmacol 6: 82, 2015.
45. Jones EM, Lubock NB, Venkatakrishnan AJ, Wang J, Tseng AM, Paggi JM, Latorraca NR, Cancilla D, Satyadi M, Davis JE, *et al*: Structural and functional characterization of G protein-coupled receptors with deep mutational scanning. Elife 9: e54895, 2020.
46. Xie L, Xiao K, Whalen EJ, Forrester MT, Freeman RS, Fong G, Gygi SP, Lefkowitz RJ and Stamler JS: Oxygen-regulated beta(2)-adrenergic receptor hydroxylation by EGLN3 and ubiquitylation by pVHL. Sci Signal 2: ra33, 2009.
47. Kertesz V, Weiskittel TM, Vavrek M, Freddo C and Van Berkel GJ: Extraction efficiency and implications for absolute quantitation of propranolol in mouse brain, liver and kidney tissue sections using droplet-based liquid microjunction surface sampling high-performance liquid chromatography/electrospray ionization tandem mass spectrometry. Rapid Commun Mass Spectrom 30: 1705-1712, 2016.
48. Wu Y, Zhang K, Jiang N, Chen Z, Sun X, Zha H, Lin M, Li J, Pan X, Chen J, *et al*: Iron-fueled ferroptosis: a new axis for immunomodulation to overcome cancer drug resistance-from immune microenvironment crosstalk to therapeutic translation. Front Immunol 16: 1726210, 2025.
49. Pan D, Jiao M, Zhu Y, Hu M, Li F, Yu J and Li CY: DGAT1 inhibition induces ferroptosis and enhances cancer immunotherapy efficacy. Cancer Res: Mar 11, 2026 (Epub ahead of print).
50. Haoyue W, Kexiang S, Shan TW, Jiamin G, Luyun Y, Junkai W and Wanli D: Icariin promoted ferroptosis by activating mitochondrial dysfunction to inhibit colorectal cancer and synergistically enhanced the efficacy of PD-1 inhibitors. Phytomedicine 136: 156224, 2025.
51. Lebelo MT, Joubert AM and Visagie MH: Warburg effect and its role in tumourigenesis. Arch Pharm Res 42: 833-847, 2019.
52. Ma S, Zhang X, Fan J, Chen M, Yao Q, Zhang N, Shi K, Duan M, Yang H, Gao T, *et al*: DUSP1-mediated suppression of p38 MAPK signaling pathway reduces ferroptosis in cerebral ischemia-reperfusion injury. Neurochem Int 189: 106024, 2025.
53. Kang Y, Nagaraja AS, Armaiz-Pena GN, Dorniak PL, Hu W, Rupaimoole R, Liu T, Gharpure KM, Previs RA, Hansen JM, *et al*: Adrenergic stimulation of DUSP1 impairs chemotherapy response in ovarian cancer. Clin Cancer Res 22: 1713-1724, 2016.
54. Bex A, Ghanem YA, Albiges L, Bonn S, Campi R, Capitanio U, Dabestani S, Hora M, Klatte T, Kuusk T, *et al*: European association of urology guidelines on renal cell carcinoma: The 2025 update. Eur Urol 87: 683-696, 2025.
55. Motzer RJ, Jonasch E, Agarwal N, Alva A, Bagshaw H, Baine M, Beckermann K, Carlo MI, Choueiri TK, Costello BA, *et al*: NCCN Guidelines® Insights: Kidney cancer, version 2.2024. J Natl Compr Canc Netw 22: 4-16, 2024.
56. Louandre C, Ezzoukhry Z, Godin C, Barbare JC, Mazière JC, Chauffert B and Galmiche A: Iron-dependent cell death of hepatocellular carcinoma cells exposed to sorafenib. Int J Cancer 133: 1732-1742, 2013.
57. Dixon SJ, Patel DN, Welsch M, Skouta R, Lee ED, Hayano M, Thomas AG, Gleason CE, Tatonetti NP, Slusher BS and Stockwell BR: Pharmacological inhibition of cystine-glutamate exchange induces endoplasmic reticulum stress and ferroptosis. Elife 3: e02523, 2014.
58. Clark JW, Eder JP, Ryan D, Lathia C and Lenz HJ: Safety and pharmacokinetics of the dual action Raf kinase and vascular endothelial growth factor receptor inhibitor, BAY 43-9006, in patients with advanced, refractory solid tumors. Clin Cancer Res 11: 5472-5480, 2005.
59. Choueiri TK and Kaelin WG Jr: Targeting the HIF2-VEGF axis in renal cell carcinoma. Nat Med 26: 1519-1530, 2020.
60. Herselman MF, Lin L, Luo S, Yamanaka A, Zhou XF and Bobrovskaya L: Sex-Dependent Effects of Chronic Restraint Stress on Mood-Related Behaviours and Neurochemistry in Mice. Int J Mol Sci 24: 10353, 2023.